A delay damage mesomodel of laminates under dynamic loading: basic aspects and identification issues

Olivier Allix, Pierre Feissel, Pascal Thévenet

A delay damage mesomodel of laminates under dynamic loading: basic aspects and identification issues

O. Allix [a,*], P. Feissel [a], P. Thévenet [b]

[a] *LMT-Cachan, Ecole Nationale Superieure de Cachan/CNRS/Université Paris VI, 61 Avenue du Président Wilson, 94235 Cachan Cedex, France*
[b] *EADS-CCR, 12, rue Pasteur, 92152 Suresnes Cedex, France*

This paper deals with the modeling of damage in laminates under dynamic loading. In the first part, the basic aspects of the model, which were developed in previous studies, are described. In the second part, we focus on current developments concerning the identification of the model using dynamic experiments. Since the applications are related to the design of composite crash absorbers, particular attention is given to the dissipation of energy.

Keywords: Composites; Mesomodeling; Damage; Fracture; Wave propagation

1. Introduction

The design of composite crash absorbers, whose purpose is to ensure the safety of aircraft passengers in case of a crash during landing, is a challenging task. In order to avoid numerous and costly experimentations, *EADS Suresnes* wishes to develop a reliable numerical tool. Such a tool must include properly identified material models capable of capturing the physics of the deterioration and dissipation phenomena which take place during a crash.

The absorbers we are focusing on are made of continuous Kevlar–Carbon multidirectional laminates. These are characterized by a deterioration scheme involving several damage mechanisms, the most important of them being multifragmentation of the fibers, delamination and transverse cracking. In order to take these mechanisms into account, a first damage mesomodel was developed in statics. The main feature of this damage mesomodel is that it introduces the damage mechanisms through internal damage variables which are constant throughout the thickness of each ply. In addition, an interface damage model was introduced to deal with delamination [4]. In the type of loading under consideration, since fracture is always a dynamic phenomenon, high strain rates occur, particularly during the localization process. The rate effects which take place during the fracture process are modeled using a delay damage model. The main assumptions of the delay model are the following:

(i) the evolution of damage due to variations of forces is not instantaneous,
(ii) a maximum damage rate exists, just as a maximum crack velocity exists.

A key issue in the case of energy absorption is the precise identification of the energy dissipated during fracture. Usually, this is not done because the behavior, although it is well-known before localization, cannot be identified after the peak using homogeneous tests. Therefore, for dynamic loading, the problem of the identification of the model in the case of localization of strains and damage must be dealt with. One difficulty is

* Corresponding author. Tel.: +33-1-4740-2735; fax: +33-1-4740-2785.
E-mail address: allix@lmt.ens-cachan.fr (O. Allix).
URL: http://www.lmt.ens-cachan.fr.

that the boundary conditions are rarely known perfectly and often known with a great deal of imprecision when fracture occurs.

In this paper, we first review the basic aspects of the model which was developed in previous studies, first in statics [1–3], then in dynamics [5]. Next, we focus on the rate effect with special attention on the dissipated energy, both from a local point of view and from a structural point of view. Finally, we propose an identification strategy which is quite insensitive to the uncertainties on the boundary conditions and we illustrate this strategy with simple but representative examples.

2. Damage mechanics and mesomodeling of laminates

When dealing with composites, the key issue is the scale on which the model is constructed. This is also the scale on which the calculations have to be performed. On the one hand, the use of the microscale, besides numerous other difficulties, would raise the computing costs beyond reasonable limits. On the other hand, the use of the macroscale would not enable a proper representation of the basic features of the laminate and of its deterioration mechanism. Moreover, for severe dynamic loading, the concept of homogenized material is meaningless. Therefore, it is necessary to define a scale on which the material can be described properly without going into excessive detail. A pragmatic approach consists of determining a characteristic length of the main damage mechanisms. For laminated composites, between the macroscale of the structure and the microscale of the single fiber, there is an intermediate modeling scale called the mesoscale. This scale is associated with the thickness of the layer and the thicknesses of the different interlaminar interfaces. On this scale, the main damage mechanisms (delamination, matrix microcracking, fiber/matrix debonding and fiber breakage) appear nearly uniform throughout the thickness of each mesoconstituent, at least under quasi-static loading. Thus, they can be described in a relatively simple way. In our method, we conjecture that due to the smallness of the mesoscale (one-tenth of a mm) a static description of the damage mechanisms should remain valid even for high loading rates. Therefore, we are proposing to adapt a mesomodel previously defined for static loading [1–4] to the dynamic case. This mesomodel is initially defined by means of two mesoconstituents:

- a single layer, which is assumed to be homogeneous and orthotropic,
- an interface, which is a mechanical surface connecting two adjacent layers and which depends on the relative orientation of their fibers (Fig. 1).

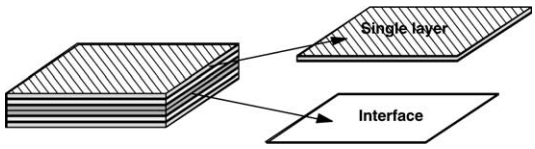

Fig. 1. Mesomodel of a laminate.

The damage mechanisms are taken into account by means of internal damage variables. Then, a mesomodel is defined by adding another property which consists of prescribing a uniform damage state throughout the thickness of the elementary ply; this point plays a major role when one tries to simulate a crack with a damage model. Additionally, delay damage models are introduced. One limitation of the proposed mesomodel is that material fracture is described by only two types of macrocracks: (i) delamination cracks within the interfaces and (ii) cracks orthogonal to the laminate's midplane, each cracked layer being cracked throughout its thickness.

2.1. The single-layer model

Let us consider the case of a laminated SiC/MAS-L composite with silicon carbide fibers and a glass matrix. This material is produced by the French company *EADS*. The stiffness of the fiber (200 GPa) is greater than that of the matrix (75 GPa) and cracks appear first in the matrix. This material was modeled and characterized for static loading in [3] based on previous studies on carbon-epoxy laminates [2]. Each layer is reinforced in only one direction. In the following expressions, subscripts 1, 2 and 3 designate the fiber's direction, the transverse direction within the layer and the normal direction respectively. Three scalar damage variables, assumed to be constant throughout the thickness of the ply, are used: d_1, associated with cracks orthogonal to the fiber's direction; d_2 and d_{12}, associated with cracks parallel to the fiber's direction.

2.1.1. Damage kinematics

The model is defined to be consistent with two experimental observations:

- the behavior in tension and the behavior in compression are independent;
- the ratio between v_{12}^0 and E_1^0 is constant.

Moreover, the damage related to out-of-plane stresses is taken into account only in the interface model. Thus, the expression of the strain energy density of the damaged elementary layer is:

$$E_D = \frac{1}{2}\left[\frac{\langle\sigma_{11}\rangle_+^2}{E_1^0(1-d_1)} + \frac{\langle-\sigma_{11}\rangle_+^2}{E_1^0} - 2\frac{\nu_{12}^0}{E_1^0}\sigma_{11}\sigma_{22} - 2\frac{\nu_{13}^0}{E_1^0}\sigma_{11}\sigma_{33} + \frac{\langle\sigma_{22}\rangle_+^2}{E_2^0(1-d_2)} + \frac{\langle-\sigma_{22}\rangle_+^2}{E_2^0} - 2\frac{\nu_{23}^0}{E_2^0}\sigma_{22}\sigma_{33} + \frac{\sigma_{33}^2}{E_3^0} + \frac{\sigma_{12}^2}{G_{12}^0(1-d_{12})} + \frac{\sigma_{13}^2}{G_{13}^0} + \frac{\sigma_{23}^2}{G_{23}^0}\right] \quad (1)$$

where $\langle\cdot\rangle_+$ designates the positive part. This expression enables us to distinguish between tension and compression depending on whether the cracks are closed or open. The rates of release of damage energy associated with d_1, d_2 and d_{12} are expressed as follows:

$$\begin{cases} Y_1 = \frac{\partial\langle E_D\rangle}{\partial d_1}\Big|_\sigma = \frac{\langle\langle\sigma_{11}\rangle_+^2\rangle}{2E_1^0(1-d_1)^2} \\ Y_2 = \frac{\partial\langle E_D\rangle}{\partial d_2}\Big|_\sigma = \frac{\langle\langle\sigma_{22}\rangle_+^2\rangle}{2E_2^0(1-d_2)^2} \\ Y_{12} = \frac{\partial\langle E_D\rangle}{\partial d_{12}}\Big|_\sigma = \frac{\langle\sigma_{12}^2\rangle}{2G_{12}^0(1-d_{12})^2} \end{cases} \quad (2)$$

where $\langle\!\langle\cdot\rangle\!\rangle$ designates the mean value through the thickness.

2.1.2. Damage evolution in statics

For the sake of simplicity, the behavior in the fiber's direction is assumed to be independent on the transverse and shear behavior. Moreover, through the material parameter b, the model introduces a coupling between the evolution of d_2 and that of d_{12}, which, on the average, are both associated with the same types of cracks. Then, the damage evolution is given by:

$$\begin{cases} d_1 = f_1(\sqrt{\underline{Y_1}}) & \text{if } d_1 < 1,\ d_1 = 1 \text{ otherwise} \\ d_2 = f_2(\sqrt{\underline{Y_{12}} + b\underline{Y_2}}) & \text{if } d_2 < 1,\ d_2 = 1 \text{ otherwise} \\ d_{12} = f_{12}(\sqrt{\underline{Y_{12}} + b\underline{Y_2}}) & \text{if } d_{12} < 1,\ d_{12} = 1 \text{ otherwise} \end{cases} \quad (3)$$

where $\underline{Y} = \sup_{\tau\leqslant t} Y|_\tau$ for each quantity Y.

The static identification of these evolution laws (i.e. the identification of functions f_1, f_2 and f_{12}) is carried out by macrotests in tension–compression on different stacking sequences of the laminate [3]. Then, the classical theory of laminates is used to obtain information on the elementary ply's scale. For example, Fig. 2 shows the results of the tension–compression test on the unidirectional specimen and Fig. 3 shows the evolution law of d_1 vs. Y_1.

2.2. Modeling of the interlaminar interface [4,8]

2.2.1. Definition of the interface

The interface is a mechanical surface which carries out stress and displacement transfers from one ply to another. It depends on the relative orientations of the

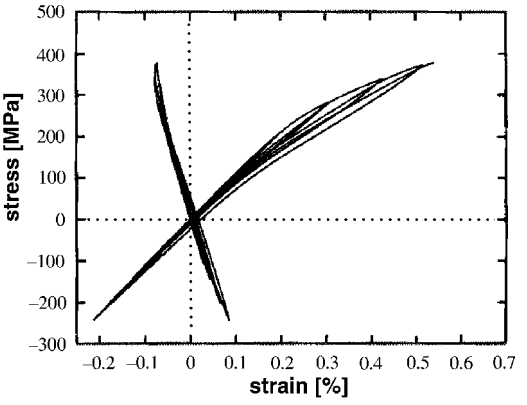

Fig. 2. Tension-compression test on unidirectional SiC/MASL.

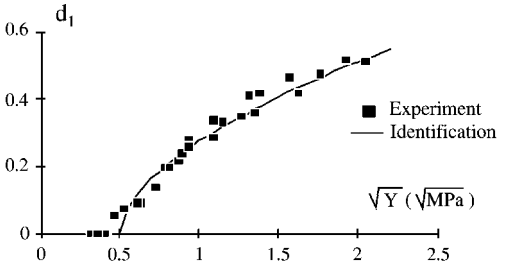

Fig. 3. Static damage evolution law $d_1 = f_1(\sqrt{Y_1})$.

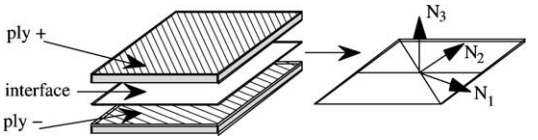

Fig. 4. The orthotropic directions of the interface.

upper and lower plies. We assume that it is orthotropic. The axes $\boldsymbol{N}_1$ and $\boldsymbol{N}_2$ are the bisectors of the angle between the directions of the fibers of the adjacent layers (see Fig. 4).

The kinematic variable is the displacement discontinuity designated by:

$$[\![\boldsymbol{U}]\!] = \boldsymbol{U}^+ - \boldsymbol{U}^- = [\![U_1]\!]\boldsymbol{N}_1 + [\![U_2]\!]\boldsymbol{N}_2 + [\![U_3]\!]\boldsymbol{N}_3 \quad (4)$$

The undamaged energy of the interface is:

$$E_D = \frac{1}{2}\left[k_1^0[\![U_1]\!] + k_2^0[\![U_2]\!] + k_3^0[\![U_3]\!]\right] = \frac{1}{2}\left[\frac{\sigma_{13}^2}{k_1^0} + \frac{\sigma_{23}^2}{k_2^0} + \frac{\sigma_{33}^2}{k_3^0}\right] \quad (5)$$

where k_1^0, k_2^0 and k_3^0 are the initial elastic characteristics.

2.2.2. Kinematics and damage evolution

The interface damage model is built using the same approach as for the single-layer model. The deterioration of the interface can be described by three damage variables:

$$E_{\mathrm{D}} = \frac{1}{2}\left[\frac{\langle\sigma_{33}\rangle_+^2}{k_3^0(1-d_3)} + \frac{\langle-\sigma_{33}\rangle_+^2}{k_3^0} + \frac{\sigma_{13}^2}{k_1^0(1-d_{13})} + \frac{\sigma_{23}^2}{k_2^0(1-d_{23})}\right] \tag{6}$$

The forces associated with the dissipation are:

$$\begin{cases} Y_3 = \left.\frac{\partial E_{\mathrm{D}}}{\partial d_3}\right|_\sigma = \frac{\langle\sigma_{33}\rangle_+^2}{2k_3^0(1-d_3)^2} \\ Y_{13} = \left.\frac{\partial E_{\mathrm{D}}}{\partial d_{13}}\right|_\sigma = \frac{\sigma_{13}^2}{2k_1^0(1-d_{13})^2} \\ Y_{23} = \left.\frac{\partial E_{\mathrm{D}}}{\partial d_{23}}\right|_\sigma = \frac{\sigma_{23}^2}{2k_2^0(1-d_{23})^2} \end{cases} \tag{7}$$

A simple modeling approach consists in considering that the evolution of damage is governed by the equivalent damage force:

$$Y = Y_3 + \gamma_1 Y_{13} + \gamma_2 Y_{23} \tag{8}$$

where γ_1 and γ_2 are constant coupling parameters. With respect to the delamination modes, these terms are associated with the first, second and third opening modes respectively. The damage evolution law is defined by:

$$\begin{cases} d = d_3 = d_{13} = d_{23} = w(\sqrt{\underline{Y}}) & \text{if } d < 1 \\ d = d_3 = d_{13} = d_{23} = 1 & \text{otherwise} \end{cases} \tag{9}$$

2.3. Modeling of the delay damage effect

It is well-known that classical damage models are incapable of describing fracture properly. Consequently, the numerical simulation of failure initiated by strain softening depends to a great extent on the mesh being used [7]. One way of avoiding such numerical difficulties is to use localization limiters [9]. This is a regularization procedure based on the introduction of additional terms in the formulation of the continuum. A large class of these limiters was studied by Sluys [14]. For example, the non-local theory [10] or the second-gradient approach include higher-order gradient terms. Alternatively, the use of a material's rate dependence in the constitutive model introduces an implicit length scale into the governing equations of the problem and removes mesh sensitivity [11,12]. In order to respect the localization size, one often has to introduce a characteristic time that is not related to any physical phenomenon.

Now, the problem consists in proposing and identifying a physically meaningful damage model which provides a consistent prediction of fracture. Of course, such a model depends to a great extent on the type of material under consideration. In particular, the length scale being introduced is related to the material's internal length scales (i.e. its heterogeneity). This was the concept which governed the damage mesomodel described previously. The model presented here is then completed by introducing a viscosity on the damage evolution law. Furthermore, it is assumed that the damage rate is necessarily finite, that is rupture is not instantaneous. As a consequence, the delay damage model is defined by introducing a maximum damage rate or a minimum critical time explicitly. The latter, being a characteristic of the local fracture process itself, is several orders of magnitude smaller than the characteristic time associated with classical viscoelasticity or viscoplasticity models. Another point, that is not taken under consideration here, is that, certain composites, e.g. glass-epoxy laminates, are eminently viscous, which obviously influences their dynamic response. However, the characteristic times introduced in such cases are not related to the fracture process.

In order to investigate the performance of our damage model with delay effects, let us consider a one-dimensional case. The analysis is based on a simple damage model with only one scalar damage variable defined as the relative variation of the elastic modulus

$$\sigma = E^0(1-d)\langle\epsilon\rangle_+ - E^0\langle-\epsilon\rangle_+ \tag{10}$$

The model is defined by its strain energy E_{D}, which is divided into two parts in reference to the fact that the cracks can be closed or open:

$$E_{\mathrm{D}} = \frac{1}{2}\left[\frac{\langle\sigma\rangle_+^2}{E^0(1-d)} + \frac{\langle-\sigma\rangle_+^2}{E^0}\right] \tag{11}$$

The damage energy release rate is:

$$Y = \left.\frac{\partial E_{\mathrm{D}}}{\partial d}\right|_\sigma = \frac{\langle\sigma\rangle_+^2}{2E^0(1-d)^2} = \frac{E^0\langle\epsilon\rangle_+^2}{2} \tag{12}$$

The evolution of damage is assumed to be driven by Y. In fact, for many long-fiber composites [2,3] and for a progressive damage mode, a typical quasi-static damage evolution law is:

$$\begin{cases} d = \langle f(\sqrt{\underline{Y}})\rangle_+ & \text{if } d < 1 \\ d = 1 & \text{otherwise} \end{cases} \quad \text{with} \quad \begin{cases} \underline{Y} = \sup_{\tau\le t} Y|_\tau \\ f(\sqrt{Y}) = \frac{\sqrt{Y}-\sqrt{Y_0}}{\sqrt{Y_{\mathrm{c}}}-\sqrt{Y_0}} \end{cases} \tag{13}$$

In the following examples, we will assume that there is no threshold, i.e. $Y_0 = 0$, and we will also study the influence of the static law on the time to rupture and on the dissipated energy. We will choose the static law among the family of power laws given by:

$$f(\sqrt{Y}) = \left(\frac{\sqrt{Y}}{\sqrt{Y_{\mathrm{c}}}}\right)^n = \left(\frac{\langle\epsilon\rangle_+}{\epsilon_{\mathrm{c}}}\right)^n, \quad \text{where: } Y_{\mathrm{c}} = \frac{E^0\epsilon_{\mathrm{c}}^2}{2} \tag{14}$$

A consequence of the expression of $\underline{Y}$ is that for non-monotonic loading the damage variable depends on the maximum value of the damage force over time.

The introduction of a delay effect leads to a new damage evolution law which can be written as:

$$\dot{d} = \frac{1}{\tau_c} \cdot \{1 - H[\langle f(\sqrt{Y}) - d \rangle_+]\} \quad \text{if } d < 1,$$
$$d = 1 \text{ otherwise} \tag{15}$$

A consequence of this law is that for a quasi-static evolution of damage the static evolution law is verified:

$$\dot{d} \simeq 0 \Rightarrow d = f(\sqrt{\underline{Y}})$$

In turn, this implies that $H(0) = 1$. Moreover, let us assume that $H' < 0$ and, in order to insure that $\dot{d}_{\max} = 1/\tau_c$, let us prescribe that:

$$\lim_{x \to +\infty} H(x) = 0$$

One can observe that the faster H tends to 0, the smaller the delay effect. A simple choice for H is:

$$H(x) = \exp[-a \cdot x] \tag{16}$$

With this choice, the more or less brittle character of the damage evolution law is governed by a (Fig. 5).

The physics of this type of model is such that the damage evolution is not instantaneous, but is governed by the internal characteristic time τ_c. Moreover, a maximum damage rate $1/\tau_c$ exists. Combined with a dynamic analysis, the delay effect introduces a length-scale effect into the initial value problem, even though the constitutive equations do not contain a parameter with the dimension of a length explicitly.

The type of model being studied here has the following properties:

- it is consistent with static analysis;
- the size of the fracture process zone is comparable to the thickness of the ply.

The delay damage effect can be seen first in the stress–strain curves (Fig. 6). A significant increase in the strength parameters can be observed throughout, from the quasi-static strain rate to the high strain rates typical of impact situations. A rapid analysis of this curve shows that the dissipated energy, i.e. the area under the curve, increases with the strain rate.

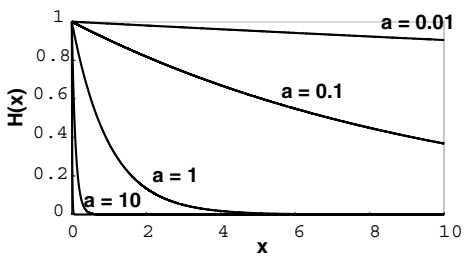

Fig. 5. Various functions for H.

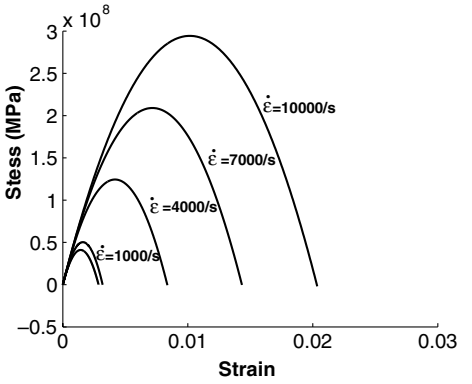

Fig. 6. The stress–strain curves for loading at various strain rates.

Previous works have already demonstrated the consistency of the damage model with delay effects for classical dynamic loading [5,6]. Before considering the consequences of the delay effect on the behavior of a structure under quasi-static loading, let us first study the influence of the loading and of the constitutive parameters on the dissipated energy and on the time to rupture.

In a first approach, we are assuming that the same values of a and τ_c can be used for the different damage modes. The objective of the following section is to study the behavior of the damage delay model precisely.

3. Strain-rate effects and dissipation analysis

The objective of this section is to study the influence, mainly on the dissipated energy, of the strain rate and delay parameters introduced in the damage evolution. We will see that the size of the localization zone is of the order of $C^0\tau_c/a$. To get a size comparable to the thickness of the ply, we chose τ_c equal to 2 μs.

The parameters of the model are given in Table 1.

3.1. Typical damage evolution in a beam until rupture

Initially, in a structure, the strain rate depends on the loading conditions and their characteristic time. Then, in the localization zone, it reaches much higher values, since localization is a dynamic phenomenon. To illustrate this strain rate effect, let us consider the one-dimensional example of a bar subjected to a moderate strain rate.

First, before localization takes place, the average strain rate is of the order of the loading parameter $\dot{\epsilon}$ and, since $\dot{\epsilon} \ll 1/\tau_c$, the damage inside the bar has the same

Table 1
Material properties

Elasticity	Damage
Young's modulus: $E^0 = 57$ GPa	Threshold: $Y_0 = 0$ MPa
Density: $\rho^0 = 2280\ \mathrm{kg\,m^{-3}}$	Critical force: $Y_c = 0.23$ MPa
Resulting quantities	Critical strain: $\epsilon_c = 2.8 \times 10^{-3}$
Wave velocity: $C^0 = 5000\ \mathrm{m\,s^{-1}}$	Delay constant: $a = 10$
Impedance: $Z^0 = 1.14 \times 10^7\ \mathrm{kg\,m^{-2}\,s^{-1}}$	Critical time: $\tau_c = 2\ \mu\mathrm{s}$

value it would have with a static law. Past the peak, the damage is localized in a band of width h in which the damage rate tends quite rapidly to $1/\tau_c$ and where the strain rate becomes much higher. In order to illustrate this point, a numerical example was calculated using an explicit scheme, starting from a static load case on a beam with an initial 1% sectional defect in the middle. The static loading was chosen such that localization would occur within a few time steps (about 1000). Fig. 7 shows the strain rate and the damage rate given by the simulation inside and outside of the localization zone.

In order to evaluate dissipation during the fracture process which takes place in the localization zone, one must:

- evaluate h,
- evaluate the strain rate in that region.

Therefore, it seems appropriate to study the effect of the strain rate on the dissipated energy in order to see where and when most of the energy absorption occurs in a loaded structure.

3.2. Estimation of the strain rate in the localization zone

From our example, we can see that the strain rate in the localization zone leads to a damage rate at rupture which is very close to $1/\tau_c$. The objective of the following section is to determine the range of strain rates in which this property is true.

3.2.1. Approximation of the damage rate for high strain rates

In this part, we are studying the response of the model to loading at a constant strain rate $\dot{\epsilon}$:

$$Y(t) = \frac{E^0 \cdot \dot{\epsilon}^2 t^2}{2}$$

For high strain rates, d is negligible compared to $f(\sqrt{Y})$, which leads to the following approximation:

$$\begin{aligned} \dot{d} &= \frac{1}{\tau_c} \cdot \left\{ 1 - \exp - a \left[\frac{\epsilon}{\epsilon_c} \right] \right\} \\ &= \frac{1}{\tau_c} \cdot \left\{ 1 - \exp - a \left[\frac{\dot{\epsilon} \cdot t}{\epsilon_c} \right] \right\} \end{aligned} \tag{17}$$

Fig. 8 shows the comparison of the previous expression with the exact one. On this example, for strain rates higher than 3000 $\mathrm{s^{-1}}$, the exact curve and the asymptotic curve nearly coincide.

Under lower strain rates, $\dot{d}$ does not reach the limit value $1/\tau_c$. Even at high strain rates, the time to rupture t_r is greater than τ_c. We need to estimate $t_r(\dot{\epsilon})$ in order to evaluate the range of strain rates in which $\dot{d} \simeq 1/\tau_c$, i.e. the range of average strain rates which are compatible with localization.

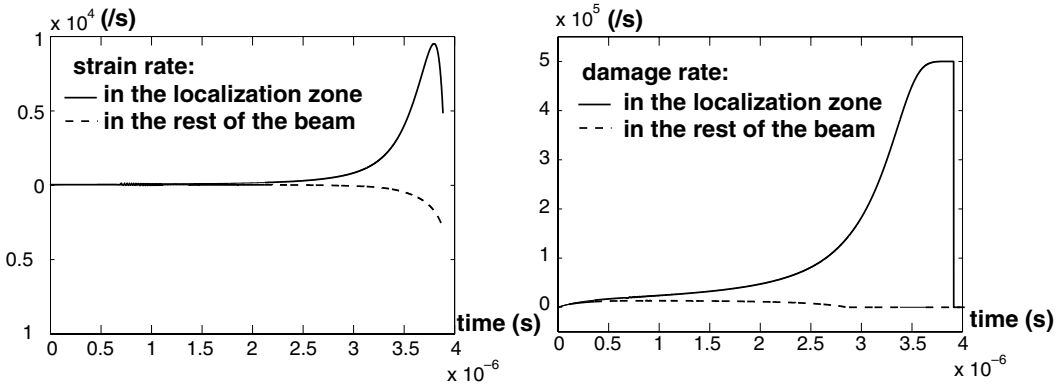

Fig. 7. Strain rate and damage rate in the beam during localization.

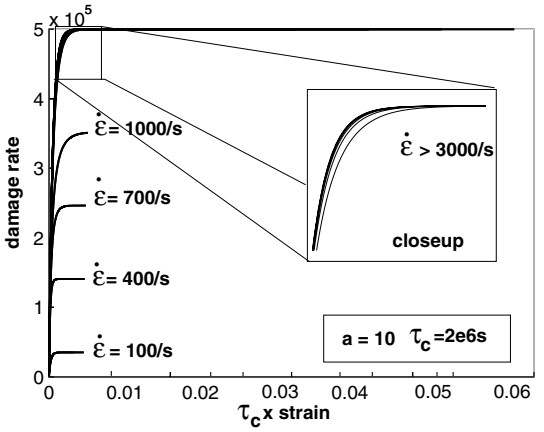

Fig. 8. Damage rate as a function of the strain; effect of the strain rate.

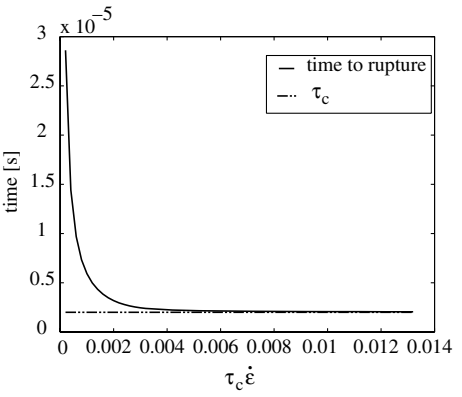

Fig. 9. Time to rupture vs. $\tau_c\dot{\epsilon}$.

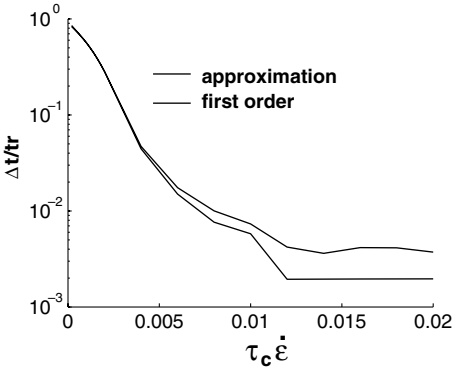

Fig. 10. Relative difference between the time to rupture and its approximations.

3.2.2. Estimation of $t_r(\dot{\epsilon})$

From (17) integrated between 0 and $\epsilon_r = \dot{\epsilon} \cdot t_r$, we get:

$$1 = \frac{1}{\dot{\epsilon}\tau_c} \cdot \left[\dot{\epsilon} \cdot t_r + \frac{\epsilon_c}{a} \cdot \left(\exp\left[-a \cdot \frac{\dot{\epsilon} \cdot t_r}{\epsilon_c} \right] - 1 \right) \right] \tag{18}$$

Let us denote:

$$t_r = \tau_c \cdot (1 + \eta) \tag{19}$$

where η is small (a few percent); therefore, we can approximate this expression by:

$$1 = 1 + \eta + \frac{\epsilon_c}{a\dot{\epsilon}\tau_c} \cdot \left[\exp\left[-a \cdot \frac{\dot{\epsilon} \cdot \tau_c}{\epsilon_c} \right] \times \left(1 - a \cdot \frac{\dot{\epsilon} \cdot \tau_c}{\epsilon_c} \eta \right) - 1 \right] \tag{20}$$

Thus,

$$\eta \simeq \frac{\epsilon_c}{a\tau_c\dot{\epsilon}} \quad \text{and} \quad t_r \simeq \tau_c + \frac{\epsilon_c}{a\dot{\epsilon}} \tag{21}$$

Now, we are able to determine $\dot{d}|_{d=1}(\dot{\epsilon}) = \dot{d}(t_r)$:

$$\dot{d} \simeq \frac{1}{\tau_c} \cdot \left\{ 1 - \exp - a \left[\frac{\dot{\epsilon}}{\epsilon_c} \cdot \tau_c(1 + \eta) - 1 \right] \right\} \tag{22}$$

In order to get $\dot{d}(t_r) \geqslant (1/\tau_c)(1 - 3 \times 10^{-4})$, $\dot{\epsilon}$ must be such that:

$$\tau_c\dot{\epsilon} \geqslant \epsilon_c \left(1 + \frac{7}{a} \right) \tag{23}$$

Verification of the quality of the approximation

Figs. 9 and 10 show respectively the exact value of $t_r(\dot{\epsilon})$ and the relative error on t_r associated with expression (17) or with its first-order approximation. Within the range of $\dot{\epsilon}$ being considered, the relative error is about 1%.

We deduce from expression (22) that the minimum strain rate in the localization zone is:

$$\tau_c\dot{\epsilon} = \epsilon_c \left(1 + \frac{7}{a} \right) \simeq 6 \times 10^{-3} \tag{24}$$

Fig. 8 shows that this approximation is very satisfactory.

3.2.3. Estimation of the density of dissipated energy

In the general case, the expression of the density of dissipated energy is:

$$\omega_d = \int_0^{t_r} Y \cdot \dot{d}\delta t, \quad \text{with: } t_r \text{ being the time to rupture} \tag{25}$$

For a uniform strain rate, we get:

$$\omega_d = \int_0^{t_r} \frac{E^0 \cdot \dot{\epsilon}^2}{2} \cdot t^2 \cdot \dot{d}(t)\delta t = \frac{E^0}{2\dot{\epsilon}} \int_0^{\epsilon_r(\dot{\epsilon})} \epsilon^2 \cdot \dot{d}(\epsilon)\delta\epsilon \tag{26}$$

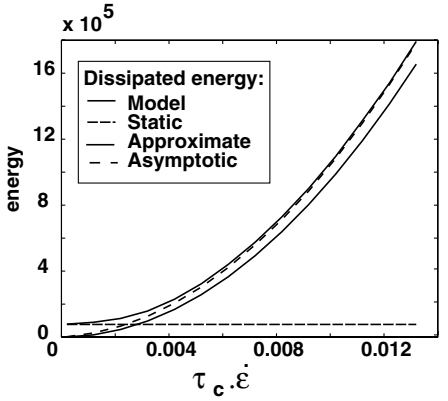

Fig. 11. Dissipated energy vs. $\tau_c\dot{\epsilon}$.

In the localization zone, this expression can be approximated by:

$$\omega_d \simeq \frac{E^0 \cdot \dot{\epsilon}^2}{2 \cdot \tau_c} \cdot \frac{\tau_c^3}{3}[1+\eta]^3 \simeq \frac{E^0 \cdot (\tau_c\dot{\epsilon})^2}{6}\left[1+\frac{3\epsilon_c}{a\tau_c\dot{\epsilon}}\right] \tag{27}$$

which, itself, can be approximated by:

$$\omega_d \simeq \frac{E^0 \cdot (\tau_c\dot{\epsilon})^2}{6} \tag{28}$$

Fig. 11 shows the exact value of ω_d and its approximate values according to (27) and (28). It appears that in the localization zone ω_d varies like $(\tau_c\dot{\epsilon})^2$, which, taking (22) into account, leads to:

$$\omega_d \simeq \frac{E^0}{6}\epsilon_c^2\left(1+\frac{7}{a}\right)^2 = \omega_s\left(1+\frac{7}{a}\right)^2 \tag{29}$$

where ω_s is the static density of dissipated energy. In turn, this expression provides a means of identifying a.

4. Estimation of the width of the localization zone: one-dimensional wave propagation analysis

Let us consider a bar of infinite length whose material behaves according to the delay damage model presented above. The bar is assumed to be subjected to uniform quasi-static loading and its homogeneous state is characterized by $\underline{d}$, $\underline{\epsilon}$ with $\underline{\epsilon} = \underline{d}\epsilon_c$ for the model being studied.

Now, let us consider, as in e.g. [14] or [15], the equation of motion linearized about the homogeneous strained state $(\underline{\epsilon}, \underline{d})$:

$$\dot{\sigma}_{,x} = \rho\ddot{v} \quad \text{with } \dot{\sigma} = E\left[(1-\underline{d})\dot{\epsilon} - \dot{d}\underline{\epsilon}\right] \tag{30}$$

and, observing that $\dot{\epsilon}_{,x} = v_{,xx}$ (where v denotes the velocity perturbation):

$$c_0^2\left[(1-\underline{d})v_{,xx} - \dot{d}_{,x}\underline{\epsilon}\right] = \ddot{v} \quad \text{with } c_0 = \sqrt{\frac{E}{\rho}} \tag{31}$$

Linearizing the damage evolution law around the strained static state yields:

$$\ddot{d} = \frac{a}{\tau_c}\left(\frac{\dot{\epsilon}}{\epsilon_c} - \dot{d}\right) = \frac{1}{T_c}\left(\frac{\dot{\epsilon}}{\epsilon_c} - \dot{d}\right) \quad \text{with } T_c = \frac{\tau_c}{a} \tag{32}$$

Now, let us consider perturbations of the harmonic form:

$$\begin{cases} v = v_0 \exp i(\omega t - kx) \\ \dot{d} = \dot{d}_0 \exp i(\omega t - kx) \end{cases} \tag{33}$$

where k is complex due to the viscosity induced by the delay damage model.

The introduction of the wave expression into the linearized problem leads to the following system:

$$\begin{cases} \left[(1-\underline{d})k^2 - \frac{\omega^2}{c_0^2}\right]v_0 + [ik\underline{\epsilon}]\dot{d}_0 = 0 \\ \left[\frac{ik}{T_c\epsilon_c}\right]v_0 + \left[\frac{1}{T_c} + i\omega\right]\dot{d}_0 = 0 \end{cases} \tag{34}$$

For a non-trivial solution corresponding to a zero determinant of the above system to exist, the following dispersion equation must be verified:

$$(c_0T_ck)^2 = (T_c\omega)^2 \times \frac{(1-2\cdot\underline{d}) + (T_c\omega)^2(1-\underline{d}) - i\underline{d}T_c\omega}{(1-2\cdot\underline{d})^2 + (T_c\omega)^2(1-\underline{d})^2} \tag{35}$$

This expression yields the values of the real and imaginary parts of the wave vector. In the following expressions, we designate by $\underline{\omega}$ and $\underline{k}$ the non-dimensional frequency and wave vector respectively, i.e.:

$$\begin{aligned} \underline{\omega} &= T_c\omega \\ \underline{k} &= c_0T_ck = \beta + i\alpha \end{aligned} \tag{36}$$

α represents the rate of decay of the solution and its inverse represents the non-dimensional length of energy concentration for a given $\underline{\omega}$.

From (35), one can deduce:

$$\begin{aligned} \beta^2 &= P\left(\sqrt{a^2+b^2} + a\right) \\ \alpha^2 &= P\left(\sqrt{a^2+b^2} - a\right) \end{aligned} \tag{37}$$

with:

$$\begin{aligned} P &= \frac{1}{2}\frac{\underline{\omega}^2}{(1-2\cdot\underline{d})^2 + \underline{\omega}^2(1-\underline{d})^2} \\ a &= (1-2\cdot\underline{d}) + \underline{\omega}^2(1-\underline{d}) \\ b &= -\underline{d}\underline{\omega} \end{aligned} \tag{38}$$

One can deduce from the last expression the values of c_e (which is the non-dimensional phase celerity), c_g (which

is the non-dimensional group celerity) and also the non-dimensional localization length $1/\alpha$ as a function of $\underline{\omega}$. One also gets the asymptotic value (for $\underline{\omega} \to \infty$) as a function of $\underline{d}$:

$$c_e(\infty) = c_g(\infty) = \sqrt{1-\underline{d}}$$
$$\frac{1}{\alpha(\infty)} = \frac{2(1-\underline{d})^{3/2}}{\underline{d}} \tag{39}$$

These functions are plotted in Figs. 12 and 13 for $\underline{d} = 0.6$, which is greater than the critical value of $\underline{d}$ for purely static loading, which corresponds to a change of regime. Fig. 14 presents the localization length as a function of the damage.

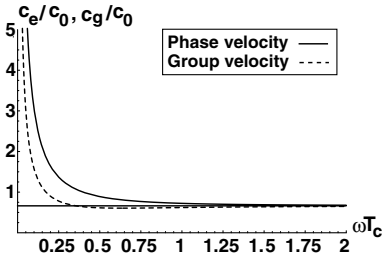

Fig. 12. Velocity $\underline{d} = 0.6$.

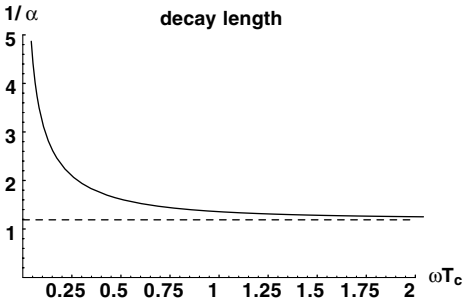

Fig. 13. Decay length $\underline{d} = 0.6$.

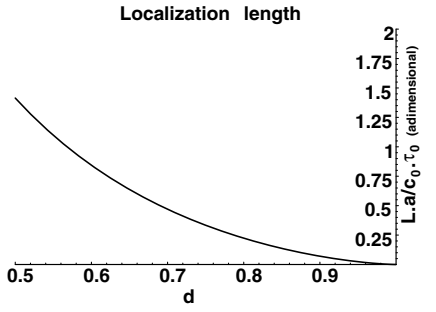

Fig. 14. Localization length.

In our example, this leads to an estimation of the width of the localization band equal to:

$$l_c = \sqrt{2} c_0 T_c \simeq 1 \text{ mm} \tag{40}$$

4.1. Dissipation in a beam

As we saw in the one-dimensional example of a beam, there are two regions in the structure: the localization zone and the rest, which behaves more or less as in statics. The previous sections provided some evaluations of both the density of dissipated energy and the width of the localization zone. A first attempt at comparing the dissipations in these two regions of the beam can consist of using these approximations. First, one can assume that the dissipated energy in the non-localized zone is the same as in statics. Then, in order to evaluate the energy dissipated in the localization zone, one can use the results of Parts 3.2.3 to get the dissipation density and (40) to evaluate the size of the localization zone.

Another remark is that the strain rate in the localization zone becomes high only after instability occurs, i.e. after a critical amount of damage (with our model parameters, this value is about $d = 1/2$). Consequently, the dissipated energy which corresponds to the localization needs to be estimated only from that time onward.

Using these approximations, Fig. 15 shows the comparison of the magnitudes of the different energies as functions of a in a 15 cm long beam. One can observe that the dissipation in the localization zone is of the same order of magnitude as the other energies for usual values of a. Therefore, it seems reasonable to identify this quantity. This approach is quite simplified, but it could explain the behavior for small values of a.

5. Identification from structural tests

The previous section focused on the dissipated energy in the localization zone. This dissipation appeared to be of the same order of magnitude as the other energies in the structure. Therefore, it seems possible to identify the related phenomena. The next question is to see how one can identify the delay damage parameters from experiments with measurement uncertainties, a situation which happens often in dynamic tests, especially when fracture is involved. In this section, we present a method based on the modified error in constitutive relation. In the case of vibration with damping, this approach was shown to be very robust [16,17]. So far, it has not been used in the case of transient dynamics. In fact, as we will show in the following section, this case involves the resolution of a coupled direct-retrograde wave propagation problem. So far, in order to test the interest of this method, we have studied only an elastic case. In this case, the information considered to be reliable is:

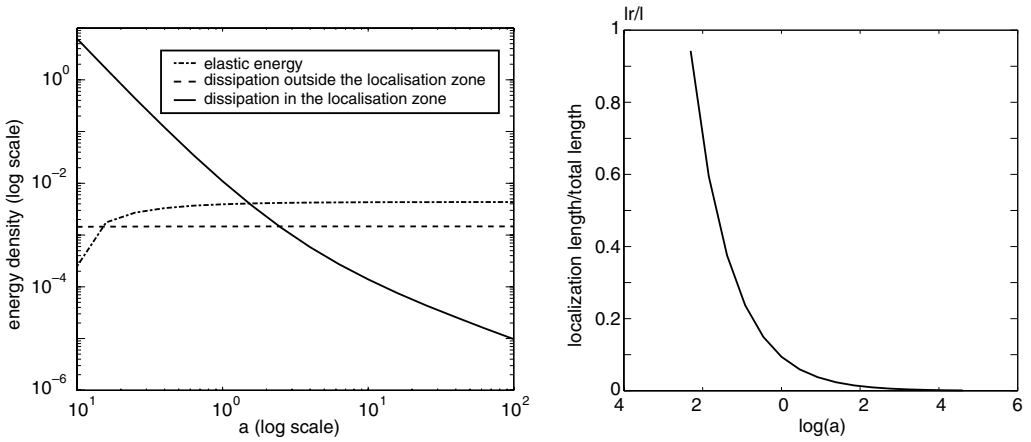

Fig. 15. Approximate energies in a beam.

- the wave equation

and the unreliable information is:

- the Young's modulus (which is to be identified),
- the boundary conditions.

5.1. The identification problem

The problem we are attempting to solve is the following: in the case of a one-dimensional elastic rod, we want to identify the Young's modulus E using a dynamic test in which one can measure both the force and the displacement boundary conditions at both ends (Fig. 16). This can be achieved with a split Hopkinson's pressure bar test. Furthermore, we assume that these boundary conditions are measured with high uncertainty. Since this is a dynamic test, the stress state in the specimen is not homogeneous and the identification must be performed by an inverse approach.

The first point to be noted is that due to the redundant boundary conditions this problem is ill-posed, i.e. it has no solution in most cases. The method we are proposing consists of first reformulating the problem so it becomes well-posed, then identifying E using the solution fields to evaluate the quality of the Young's modulus.

5.2. Formulation and resolution

Our guiding principle, which was inspired directly by studies on model updating in vibration problems [16], is

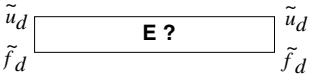

Fig. 16. The rod with redundant measurements.

Table 2
Reliable and uncertain quantities

Reliable	Uncertain
Equilibrium: $\rho \cdot \ddot{\boldsymbol{u}} - \mathrm{div}\sigma = 0$	Constitutive relation: $\sigma = E \cdot \epsilon$
	Measurements: $\tilde{\boldsymbol{u}}_\mathrm{d}$ and $\tilde{f}_\mathrm{d}$

to concentrate, during the identification process, on the exact verification of the properties which are considered to be reliable. Then, the uncertain quantities are taken into account by minimizing a modified constitutive relation error [17]. Here, let us split the quantities into two groups as shown in Table 2.

The identification of the Young's modulus E is carried out in two steps: first, for a fixed E, the ill-posed problem is reformulated as the minimization of:

$$e(u,\sigma,u_\mathrm{d},f_\mathrm{d}) = \|\sigma - E\cdot\epsilon\|^2 + \|f_\mathrm{d} - \tilde{f}_\mathrm{d}\|^2 + \|u_\mathrm{d} - \tilde{\boldsymbol{u}}_\mathrm{d}\|^2 \tag{41}$$

under the conditions:

$$u \text{ KA to } u_\mathrm{d}, \quad \sigma \text{ DA to } f_\mathrm{d}, \quad \rho\cdot\ddot{\boldsymbol{u}} - \mathrm{div}\sigma = 0 \tag{42}$$

where KA and DA means respectively kinematically admissible and dynamically admissible.

One can note that the boundary conditions u_d and f_d are related to the fields used in the minimization problem and, therefore, can be different from the measured values $\tilde{\boldsymbol{u}}_\mathrm{d}$ and $\tilde{f}_\mathrm{d}$.

This minimization under constraints is performed by introducing Lagrange multipliers. The stationarity of the Lagrangian function, denoted L, leads to a differential system in time and space which connects the expected fields and the multipliers, designated by u^*. Due to the equilibrium constraint, the formulation yields some final conditions on the Lagrangian multipliers. Therefore, it is

necessary to solve a coupled dynamic problem whose unknowns are the displacement u and the multiplier u^*, with:

$$u(0) = u_0 \quad \dot{u}(0) = \dot{u}_0 \quad \text{with } u_0, \dot{u}_0 \text{ given}$$
$$u^*(T_f) = 0 \quad \dot{u}^*(T_f) = 0 \quad \text{where } T_f \text{ is the final time} \tag{43}$$

Consequently, one must solve simultaneously a direct problem and an adjoint (time-retrograde) problem which are related to one another. Different methods for solving these problems have been studied [19]. For example, one can assemble a time scheme on all the time steps, leading to a global problem in time and space. Such methods would lead to huge matrix sizes. Another option is to use the transition matrix of the system in order to express the unknown initial conditions in terms of the final prescribed conditions. The latter is the method we chose to use.

The identification of the best E is carried out using the same functional as the minimization of:

$$\min_E g(E) = \min_E e(u(E), \sigma(E), u_d(E), f_d(E)) \tag{44}$$

where $(u(E), \sigma(E), u_d(E), f_d(E))$ is the solution of (41).

Using the same functional is a great advantage if the minimization is to be performed by a gradient method. In fact, noting that:

$$L(\sigma(E), u(E), u_d(E), f_d(E), u^*(E), \lambda(E), E) = g(E) \tag{45}$$

and considering the fact that $(\sigma(E), u(E), u_d(E), f_d(E))$ are the solutions to Eq. (41), we have:

$$\frac{\partial L}{\partial \sigma} = \frac{\partial L}{\partial u} = \frac{\partial L}{\partial u^*} = \frac{\partial L}{\partial u_d} = \frac{\partial L}{\partial f_d} = 0 \tag{46}$$

Therefore, the expression of the gradient is:

$$Dg(E) \cdot q = \frac{\partial L}{\partial E} \cdot q \tag{47}$$

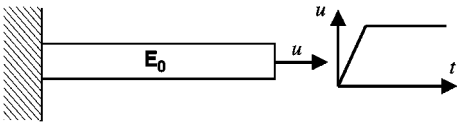

Fig. 17. The numerical test.

which can be evaluated directly from the fields which are the solutions of (41).

5.3. Example

The identification method described above was validated on a numerical example. A preliminary calculation consisted of simulating an experiment on a rod fixed at one end and subjected to a constant velocity at the other (Fig. 17).

Then, the displacements and forces at both ends were taken from this simulation in order to create a set of measurements. Some high-frequency sinusoidal perturbations (up to 40%) were added to these values to represent the uncertainties.

With these measurements, we were able to test the identification of the Young's modulus by a classical method and by the method presented here. The classical method, inspired by [18], consisted of splitting the initially ill-posed problem into two well-posed problems, one with prescribed displacements the other one with prescribed forces. The calculation was made to match the perturbed measurements exactly (Fig. 18). Then, the identification was made by defining a discrepancy between the two calculations using the solution fields. Fig. 19 shows the identification functional of each method as a function of the relative Young's modulus. On this example, our method turned out to be particularly robust whereas the other was incapable of identifying E correctly.

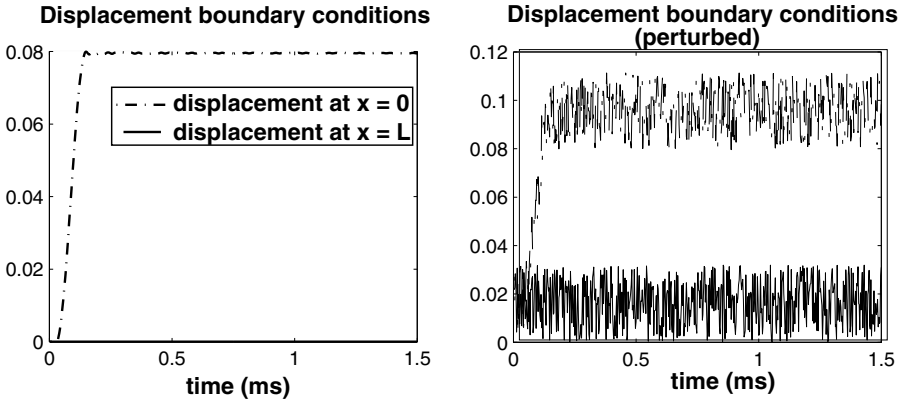

Fig. 18. Exact and perturbed boundary conditions.

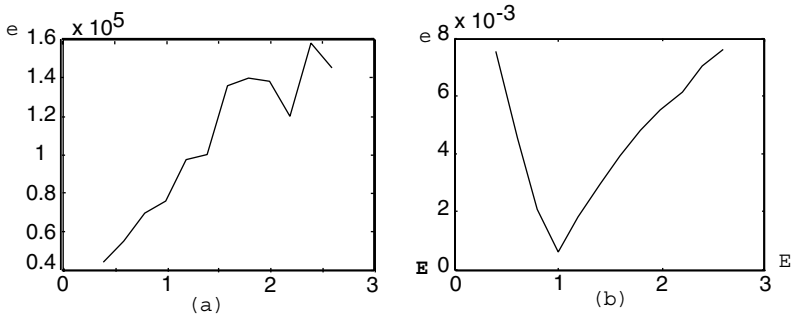

Fig. 19. Variation of the error with E: (a) classical approach, (b) our method.

In order to illustrate the numerical procedure, we show the resulting fields u and u^* in several cases:

- Using the exact boundary conditions and Young's modulus, the method yields the same displacement field as the simulation used to create the boundary conditions. u^* equals 0.
- With the exact boundary conditions and a Young's modulus different from the one to be identified, Fig. 20 shows the displacement field and the Lagrangian multiplier u^*. One can observe that u^* is different from 0, mainly because the boundary conditions are not consistent with the new wave velocity.
- For perturbed boundary conditions and the Young's modulus to be identified.
- For perturbed boundary conditions and incorrect Young's modulus.

One should note that the magnitude of the local error is governed by u^*, which explains why u^* is zero in the first case and non-zero in the others. Another remark is that due to the final conditions u^* equals 0 at the final time $T_{\max}$ (Fig. 21).

In addition, the values of u and u^* in the beam at $t = T_{\max}/2$ are shown in Fig. 22. The example with $E = 2$ and perturbed measurements shows that both imperfections influence the level of u^* and that their effects combine compared to the cases with perturbed measurements alone or with an incorrect Young's modulus alone.

Currently, we have work underway to extend this method to the case of the delay damage model. In this case, what we want to identify is the evolution law. Therefore, the static law is assumed to be known. In fact, it can be identified using standard static tests. As in the elastic case, the quantities will be divided into two groups, depending on whether we consider them to be reliable or not (Table 3).

As in the elastic case, the identification is proceeded in two steps. In the first one, the solution fields of a new mechanical problem are sought, then in the second one, the right parameters should be identified from the value of the functional for the solution fields. The problem

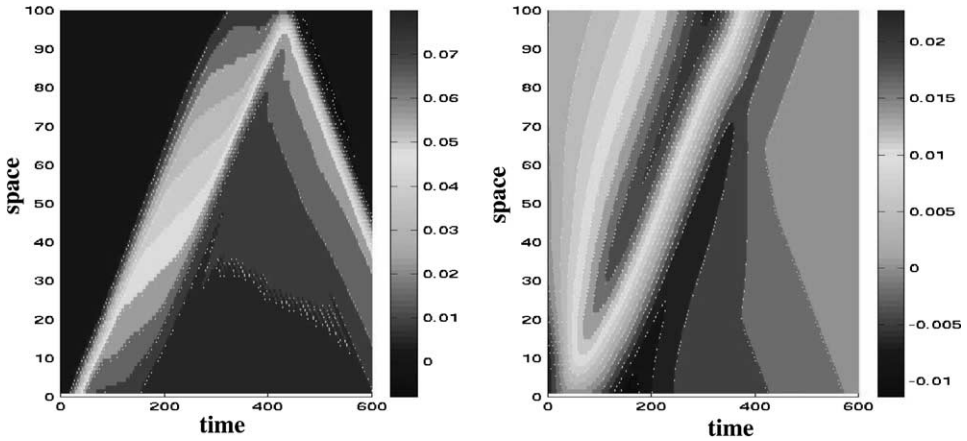

Fig. 20. u and u^* for an incorrect Young's modulus in the time x space plane.

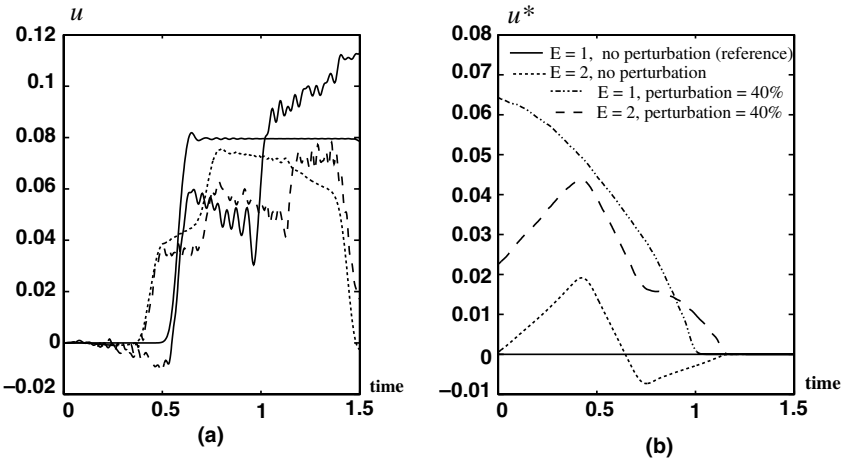

Fig. 21. Displacement u (a) and multiplier u^* (b) as functions of time in the middle of the beam.

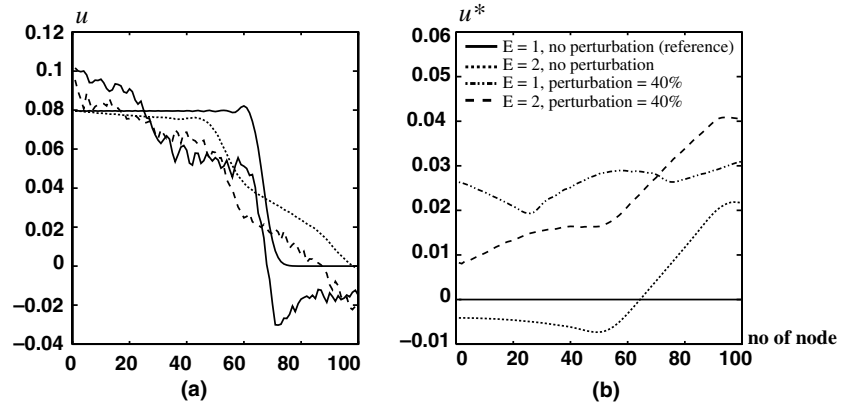

Fig. 22. Displacement in the beam at time $t = T_{\max}/2$.

Table 3
Reliable and uncertain quantities: the damage case

Reliable	Uncertain
Equilibrium: $\rho \cdot \ddot{\boldsymbol{u}} - \mathrm{div}\sigma = 0$	Evolution laws: $\dot{d} = (1/\tau_c)(1 - H(Y,d))$
Static laws: $\sigma = E \cdot (1-d) \cdot \epsilon$ $Y = E \cdot \epsilon^2/2$	Measurements: $\tilde{\boldsymbol{u}}_d$ and $\tilde{f}_d$

associated to the first step is now to find the solution fields that minimize an error in the evolution relation of the damage variable, under the constraint of equilibrium. Some difficulties, that were not encountered in the elastic case, arise. The differential system that the problem results in, becomes non-linear, with still both initial and final conditions to be satisfied. Some solving methods are still to be developed for this type of problem. Another question is the one related with the possibility of several local minima, during the identification process. If such a problem occurs, a gradient method will not be efficient anymore.

6. A three-dimensional damage calculation in dynamics

6.1. Problem definition

We present an example of a 3D finite element calculation in order to demonstrate the ability of the

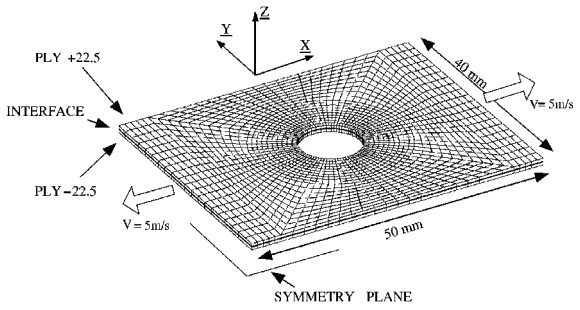

Fig. 23. Perforated laminate $[\pm 22.5]_s$ subjected to dynamic tension loading.

damage mesomodel to predict the dynamic response of a composite structure until ultimate fracture [6]. In order to perform the simulation, the constitutive damage mesomodel presented in the second section was implemented into the explicit finite element code LS-Dyna3D [20]. The following calculation was performed on a perforated SiC/MAS-L laminate $[\pm 22.5]_s$. A velocity was prescribed on two edges of the plate. After an initial ramp, the velocity was set to a constant value $V_0 = 5$ m s^{-1}. The final time ($T = 100$ μs) corresponds to a total extension of about 1 mm. The characteristics of the problem are shown in Fig. 23.

Because of the symmetry, only one-half of the structure was modeled. Let us note that reasonable values were chosen for the material constants of the interlaminar interface model. The critical times τ_c and τ_c' and the constants a and a' were given the following values:

$$\tau_c = \tau_c' = 2\ \mu s \quad \text{and} \quad a = a' = 1$$

6.2. Numerical results

Figs. 24 and 25 show the microcracking intensity maps and the fiber-direction damage maps at different times. One can see clearly that a transverse crack orthogonal to the fibers appears and then grows inside each ply. At $t = 100$ μs, the size of the transverse cracks is about 2 mm. Therefore, we can consider that final fracture occurs at about this time.

Fig. 26 shows the degradation of the $[\pm 22.5]_s$ interface. The dark area represents the completely destroyed zone and then the delamination crack.

This typical example of a progressive fracture situation illustrates the possibilities of the computational damage mesomodel. The results are in agreement with the typical degradations observed experimentally in laminates. Indeed, damage begins very close to the free surface and then propagates inside the composite.

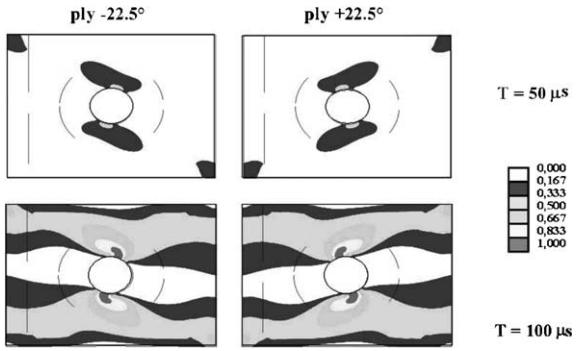

Fig. 24. Longitudinal damage maps for the layers at $t = 50$ and 100 μs.

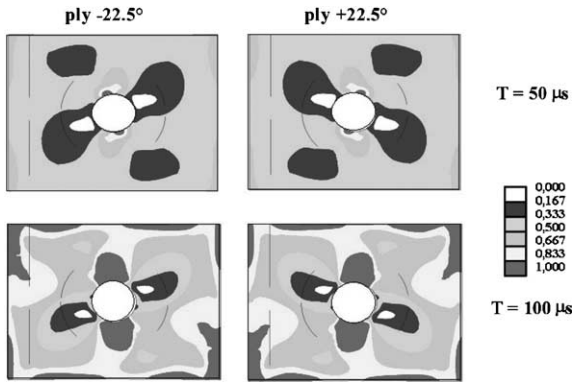

Fig. 25. Shear damage maps for the layers at $t = 50$ and 100 μs.

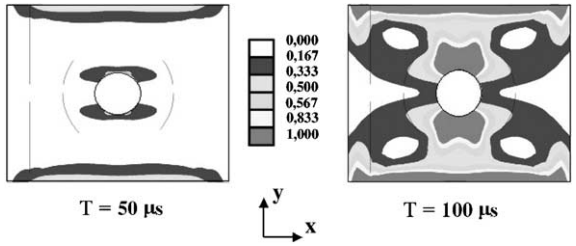

Fig. 26. Interface damage maps for the layers at $t = 50$ and $t = 100$ μs.

7. Conclusions

In this paper, a previously defined delay damage mesomodel has been studied, giving special attention to the dissipation in the localization zone which we believe to be a key factor when one deals with shock absorption.

We showed, at least for the model proposed, that this energy is quite significant and, therefore, that it should be possible to identify the delay parameters of the model.

Dynamic Hopkinson pressure bar tests, which are still in progress at *EADS*, have shown the existence of significant uncertainties on the boundary conditions. Therefore, we sought an identification approach which would be as insensitive as possible to these uncertainties. Our first results are encouraging, but should be confirmed in the case of damage with localization. This part of the work is underway.

The structural calculation presented in this paper showed the capability of such models to simulate the magnitudes of the damage mechanisms in the plies as well as in the interfaces at any time until complete fracture. The results indicate that the mesomodel reproduces the damage behavior of laminated composites qualitatively. However, the calculations performed with such a mesomodel do generate very high computation costs. Therefore, another challenge will be to develop a more effective computational strategy, possibly associated with the use of parallel computers.

References

[1] Ladevèze P. A damage computational method for composite structures. Comput Struct 1992;44:79–87.

[2] Ladevèze P, Le Dantec E. Damage modelling of the elementary ply for laminated composites. Compos Sci Technol 1992:257–67.

[3] Gasser A, Ladevèze P, Peres P. Damage modelling for a laminated ceramic composite. Materi Sci Eng 1998;250: 249–55.

[4] Allix O, Ladevèze P. Interlaminar interface modelling for prediction of laminates delamination. Compos Struct 1992;22:235–42.

[5] Allix O, Deü J-F. Delay-damage modelling for fracture prediction of laminated composites under dynamic loading. Eng Trans 1997;45:29–46.

[6] Deü J-F. Rupture des composites stratifiés sous chargement dynamique apport des méso-modèles avec endommagement retardé. Thesis of E.N.S. Cachan, France, 1997.

[7] Bazant ZP, Belytschko TB, Chang TP. Continuum theory for strain softening. J Eng Mech 1984;110:1666–92.

[8] Allix O, Lévêque D, Perret L. Identification and forecast of delamination in composite laminates by an interlaminar interface model. Compos Sci Technol 1998;58:671–8.

[9] Lasry D, Belytschko T. Localisation limiters in transient problems. Int J Solids Struct 1988;24:581–97.

[10] Pijaudier-Cabot G, Bazant ZP. Nonlocal damage theory. J Eng Mech 1987;113:1512–33.

[11] Needleman A. Material rate dependence and mesh sensitivity in localisation problems. Comput Meth Appl Mech Eng 1988;67:69–85.

[12] Loret B, Prevost JH. Dynamic strain localisation in elasto-(visco-)plastic solids, Part 1. General formulation and one-dimensional examples. Comput Meth Appl Mech Eng 1990;83:247–73.

[14] Sluys LJ. Wave propagation, localisation and dispersion in softening solids. PhD thesis, Delft University, 1992.

[15] Comi C, Perego U. Symmetric and non-symmetric nonlocal damage formulations: an assessment of merits ECCM 2001, 2001.

[16] Ladevèze P, Chouaki A. Application of a posteriori error estimation for structural model updating. Inverse Prob 1999;15:49–58.

[17] Ladevèze P. A modelling error estimator for dynamical structural model updating. In: Ladevèze P, Oden JT, editors. Advances in adaptive computational methods in mechanics. Elsevier; 1998.

[18] Rota L. An inverse approach for identification of dynamic constitutive equations. In: International symposium on inverse problems. A.A. Balkema; 1994.

[19] Feissel P, Allix O. Comportement d'absorbeur de choc en composite multicouche, modélisation et identification: identification à partir d'essais dynamiques bruités. Rapport contractuel d'avancement, EADS, 2001.

[20] Hallquist JO. LS-DYNA3D theoretical manual. Livermore Software Technology Corporation, Livermore, USA, 1993.